Polarization instability of ultrashort pulses as a source of vectorial supercontinuum

Aleksandr A. Voronin,[1,2] Il'ya V. Fedotov,[1] Jens Kobelke,[3] Matthias Jäger,[3] Kay Schuster,[3] Andrei B. Fedotov,[1,2] Hartmut Bartelt,[3,4] and Aleksei M. Zheltikov[1,2,5,*]

[1]*Physics Department, International Laser Center, M.V. Lomonosov Moscow State University, Moscow 119992, Russia*

[2]*Russian Quantum Center, Skolkovo 143025, Moscow Region, Russia*

[3]*Institute of Photonic Technology, Albert Einstein Str. 9, Jena 07745, Germany*

[4]*Friedrich Schiller University of Jena, Max-Wien-Platz 1, Jena 07743, Germany*

[5]*Department of Physics and Astronomy, Texas A&M University, College Station, Texas 77843, USA*

**Corresponding author: zheltikov@physics.msu.ru*

Received October 8, 2012; revised November 6, 2012; accepted November 6, 2012;
posted November 7, 2012 (Doc. ID 177582); published December 11, 2012

Polarization instability (PI) of ultrashort light pulses, giving rise to vectorial supercontinuum generation, is demonstrated using a subwavelength-core, highly birefringent, normally dispersive optical fiber. The evolution of ultrashort pulses in the regime of PI is shown to radically differ from polarization-instability dynamics of cw fields and longer laser pulses. As the peak power of the laser field decreases along the propagation path due to dispersion-induced pulse stretching, the Poincaré-sphere map of field dynamics is shown to evolve from the behavior typical of PI in the highly nonlinear regime toward the beating dynamics of uncoupled polarization modes, characteristic of low field intensities and cw fields. © 2012 Optical Society of America

OCIS codes: 190.7110, 320.7140.

Modulation instability (MI) is a universal scenario of nonlinear dynamics observed in a broad class of physical systems in fluid mechanics [1], plasma physics [2], nonlinear optics [3], and Bose–Einstein condensation [4]. In the MI regime, a regular wave process becomes unstable with respect to a weak modulation of the wave due the concerted action of dispersion and nonlinearity, which induces a parametric amplification of spectral sidebands, manifested in the buildup of a spiky structure on the waveform or beam profile. In optical physics, MI gives rise to a broad variety of nonlinear-optical regimes, including parametric sideband generation in optical fibers [3] and small-scale filamentation of high-power laser beams [5]. MI in highly nonlinear fibers, e.g., photonic-crystal fibers [6], enables fiber-format parametric amplification [7,8] and synthesis of tunable pulse trains [9]. In birefringent fibers, MI has been shown [10] to enable polarization-sensitive transformation of picosecond pulses, giving rise to spectral sidebands orthogonally polarized to the pump field.

In this Letter, we demonstrate polarization-sensitive MI of ultrashort light pulses, which gives rise to vectorial supercontinuum (SC) generation in a subwavelength-core, highly birefringent, normally dispersive optical fiber. The evolution of ultrashort pulses undergoing polarization instability (PI) is shown to radically differ from PI dynamics of cw fields and longer laser pulses.

To identify the key tendencies in the PI dynamics of ultrashort light pulses, we study the evolution of 100 fs near-IR laser pulses in a small-core highly birefringent fiber consisting of a germanium-doped central region surrounded by a silica cladding. The highly doped central part of the fiber has a shape of an ellipse with slow- and fast-axis radii $a_s \approx 0.55$ μm and $a_f \approx 0.30$ μm and a refractive index step of about 0.04 relative to the silica cladding. This region serves as a subwavelength index-guiding fiber core for laser pulses with a central wavelength $\lambda_0 \approx 1440$ nm used in our experiments, providing a unique combination of enhanced nonlinearity and birefringence. The nonlinear coefficient $\gamma = 2\pi\lambda^{-1}n_2S_{\text{eff}}^{-1}$ (n_2 is the nonlinear refractive index, S_{eff} is the effective mode area, and λ is the radiation wavelength) estimated for this fiber from the spectral broadening of 100 fs, 1440 nm laser pulses is $\gamma \approx 4$ kW^{-1} cm^{-1}. The phase and group birefringence for this fiber, Δn_p and Δn_g, was found from the best fit for the experimental spectra, yielding $\Delta n_p = 7 \cdot 10^{-5}$ and $\Delta n_g = 2 \cdot 10^{-6}$ at $\lambda_0 = 1440$ nm for the fundamental orthogonally polarized spatial modes. The group-velocity dispersion of the fiber is normal within the entire range of wavelengths (from 1.0 to 2.0 μm) studied in our experiments.

Our model is based on the numerical analysis of coupled generalized nonlinear Schrödinger equations (GNSEs) [3] for the guided modes of the small-core highly birefringent fiber. The model provides an accurate fit of the experimental spectra (Figs. 1 and 2) when at

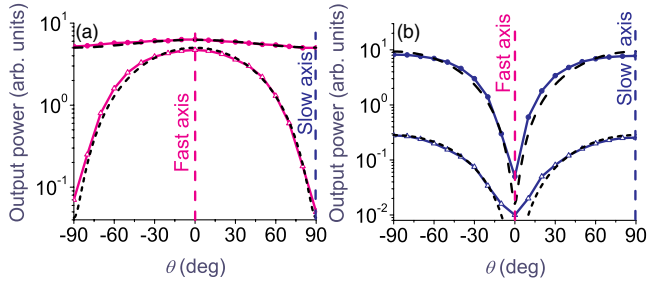

Fig. 1. (Color online) Power of ultrashort laser pulses transmitted through the fiber measured (circles and triangles) and simulated (dotted and dashed curves) as a function of the angle θ between the axis of the polarization analyzer and the fast axis of the fiber. The input laser field with $\lambda_0 = 1440$ nm and $\tau_0 = 100$ fs is polarized along the (a) fast and (b) slow fiber axis. The input pulse energy in the fundamental spatial mode E_0 is (a) 0.45 nJ (dotted curve, triangles) and 5 nJ (dashed curve, circles), (b) 0.3 nJ (dotted curve, triangles) and 4.5 nJ (dashed curve, circles).

least four guided modes are included through a joint solution of four coupled equations for two orthogonal polarization modes with two spatial modes for each polarization. For low-intensity light, strong fiber birefringence prevents polarization mode coupling, isolating these modes from each other. In this regime, the laser field polarized along either the fast ($\varphi = 0$) or the slow ($\varphi = \pi/2$) axis of the fiber retains its polarization at the fiber output [dotted curves in Figs. 1(a) and 1(b)]. In the regime of high field intensities, typical of SC generation [Figs. 2(a), 2(b), 3(a), and 3(b)], tensorial Kerr-type optical nonlinearity enhanced by the compactness of modes in the subwavelength fiber core induces anisotropic corrections to the propagation constants of polarization modes. The total mismatch of the propagation constants of the laser pump polarized along one of the fiber axes, β_p, and a weak orthogonally polarized seed (e.g., noise), β_s, is then given [3] by $\Delta\beta = \beta_p - \beta_s = \pm\pi\lambda^{-1}\Delta n_p + 2\gamma P/3$, where P is the laser peak power and the plus and minus signs correspond to the pump field polarized along the slow and fast fiber axes, respectively. While the laser field polarized along the fast fiber axis reduces fiber birefringence, the laser field polarized along the slow axis increases $|\Delta\beta|$, thus enhancing fiber birefringence. In a laser field with $\varphi = 0$ and a peak power $P_{cr} = 3\pi\Delta n_p(\lambda\gamma)^{-1}$, β_p and β_s are matched, and the polarization modes become strongly coupled. A weak seed field polarized along one of the fiber axes is amplified in this regime by a cross-polarized strong pump field [dashed curve in Fig. 1(a)], leading to a PI behavior of the fiber output and inducing well-resolved fringes in the SC spectra generated by ultrashort laser pulses in the all-normal-dispersion regime [Figs. 2(a), 2(b), and 3(a)].

In Figs. 3(a)–3(d), we present the maps of the spectral and temporal evolution along with the dynamics of the Stokes vector **S** of the laser field propagating through a highly birefringent fiber with the above-specified parameters. For ultrashort light pulses, we define the Stokes parameters as $S_1(z) = (|A_x(t_0,z)|^2 - |A_y(t_0,z)|^2)$, $S_2 = (A_x(t_0,z)A_y^*(t_0,z) + A_y(t_0,z)A_x^*(t_0,z))$, and $S_3 = i(A_y(t_0,z)A_x^*(t_0,z) - A_x(t_0,z)A_y^*(t_0,z))$, where A_x and A_y are the complex amplitudes of the polarization components of the optical field and t_0 is the instant of time corresponding to the maximum field intensity.

For a field with $P_0 \ll P_{cr}$, the trajectories of the Stokes vector lie on the Poincaré sphere with the radius $S = (S_1^2 + S_2^2 + S_3^2)^{1/2}$ in a plane parallel to S_2S_3 [curve 1 in Fig. 3(c)], with the distance between the trajectory plane and the S_2S_3 plane controlled by the initial conditions. For a pulse with $P_0 > P_{cr}$, the trajectories of the Stokes vector become essentially nonplanar [curve 2 in Fig. 3(c)], since the orthogonal polarization modes are now coupled by optical nonlinearity, but still belong to the Poincaré sphere, as S is conserved. Poincaré-sphere maps presenting polarization dynamics of ultrashort light pulses are strikingly different [curve 3 in Fig. 3(c)], combining at its initial and final stages the key features typical of polarization dynamics in high- and low-power fields. Dispersion-induced pulse stretching [Fig. 3(b)] tends to lower the peak power of ultrashort optical waveforms on a characteristic spatial scale of dispersion length. As a result, following the initial stage of strong polarization mode coupling [the IR segment in Fig. 3(c)], which is possible as long as the peak power of the laser field is higher than P_{cr}, polarization modes become effectively decoupled when the peak power of dispersion-stretched laser pulses becomes less than P_{cr} [the RX segment in Fig. 3(c)]. From this moment on, polarization modes are isolated from each other, propagating independently with no interaction and forming interference

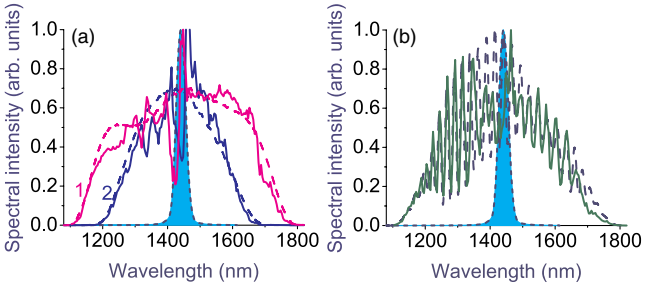

Fig. 2. (Color online) The spectra measured (solid curves) and simulated (dashed curves) at the output of the fiber with (a) $\theta = 0$ (curve 1) and $\pi/2$ (curve 2); (b) $\theta = \pi/4$. The input laser field with $\lambda_0 = 1440$ nm, $\tau_0 = 100$ fs, and $E_0 = 4$ nJ is polarized along the fast fiber axis. The input spectrum is shown by the dotted curve with shading.

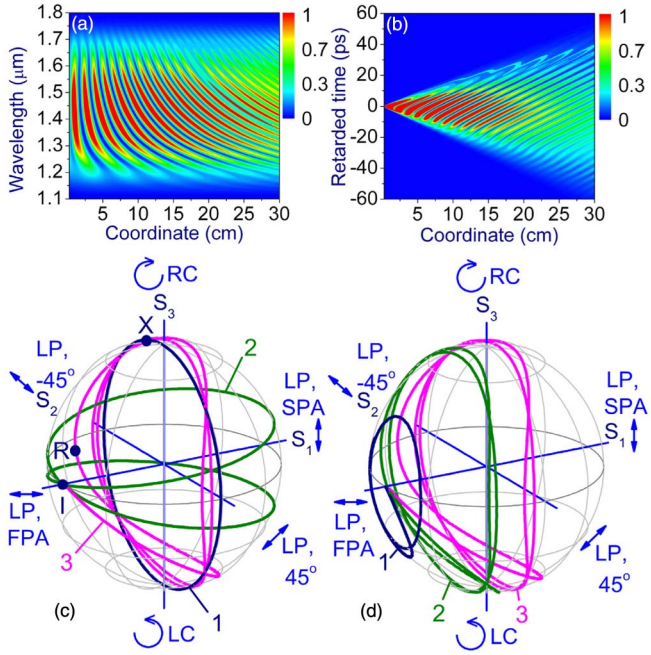

Fig. 3. (Color online) The (a) spectral and (b) temporal dynamics of a light pulse with $\tau_0 = 100$ fs, $P_0 = 35P_{cr}$, $\varphi = 0.035$, and $\theta = \pi/4$ propagating through the fiber. Poincaré-sphere maps of polarization dynamics in the same fiber for $\varphi = 0.035$ and (c) a pulse with $\tau_0 = 100$ fs and (1) $P_0 = 0.2P_{cr}$, a (2) cw field with $P_0 = 35P_{cr}$, a (3) pulse with $\tau_0 = 100$ fs and $P_0 = 35P_{cr}$ and (d) a pulse with $\tau_0 = 100$ fs, $P_0 = 35P_{cr}$, and (1) $\varphi = 0.001$, (2) $\varphi = 0.01$, and (3) $\varphi = 0.035$. Also shown are the points I and X, corresponding to the fiber input and fiber output in the experiments, and point R, where the peak power in each polarization mode becomes less than P_{cr}, as well as the Poincaré-sphere poles corresponding to an input field with a linear polarization along the fast (LP, FPA) and slow (LP, SPA) fiber axes and at an angle $\varphi = \pi/4$ (LP, 45°) and $\varphi = -\pi/4$ (LP, −45°) relative to the fast fiber axis, as well as an input field with a right- (RC) and left-hand (LC) circular polarization.

fringes in the output spectra [Figs. 2(b) and 3(a)] as they become shifted in the time domain due to the mismatch of their group velocities [Fig. 3(b)]. The fiber loss, estimated as 5% per 1 m of the fiber at 1440 nm, does not play any noticeable role in this dynamics. As a typical indication of the PI dynamics, we observe in Fig. 3(d) that small variations in the polarization state of the input field translate into greatly amplified variations in the polarization state of the fiber output.

In experiments, ultrashort light pulses were delivered by a frequency-tunable optical parametric oscillator pumped by the 800 nm, 50 fs output of a mode-locked Ti:sapphire laser. The central wavelength of laser pulses in the experiments presented below in this Letter was set at $\lambda_0 \approx 1440$ nm. The input pulse width τ_0, measured with the use of cross-correlation frequency-resolved optical gating, was equal to 100 fs. The input laser energy was varied from 0.1 to 25 nJ. The laser pulses were coupled into the fiber with a high-NA objective with a coupling efficiency of about 40%.

The symmetric spectral broadening observed at the fiber output for laser pulses with an input pulse width of about 100 fs and the central wavelength of 1440 nm [Figs. 2(a) and 2(b)] indicates the dominance of the self-phase modulation process, which is consistent with the generic scenario of spectral broadening in a normally dispersive fiber [11,12]. For a laser pulse with an input energy of 4 nJ in the fundamental spatial mode polarized along the fast fiber axis ($\varphi = 0$), the spectrum measured at the output of a 30 cm long fiber with $\theta = 0$ stretches from 1100 to 1800 nm [Fig. 2(a)]. Our GNSE-based model provides an accurate fit for the experimental spectra for different polarization arrangements [Figs. 2(a) and 2(b)]. A combination of high nonlinearity and high birefringence provided by the fiber used in our experiments allows well-resolved signatures of PI to be observed in SC spectra spanning over 100 THz. In the regime of low peak powers, the laser field polarized along either the fast ($\varphi = 0$) or the slow ($\varphi = \pi/2$) axis of the fiber retains its polarization at the fiber output [triangles in Figs. 1(a) and 1(b)]. For laser peak powers exceeding P_{cr}, polarization measurements with the input field polarized along the fast fiber axis clearly indicate that cross-polarized modes are excited in the highly birefringent fiber [circles in Fig. 1(a)]. As the input laser energy coupled to the fundamental spatial mode of the fiber is increased from 0.45 to 5 nJ, the efficiency of cross-polarized mode excitation grows from 0.8% to 45%.

The output spectrum measured with the axis of the polarization analyzer oriented along the polarization of the input field ($\theta = \varphi = 0$) is seen to be substantially broader than the spectrum of the cross-polarized component of the output field, measured with $\varphi = 0$ and $\theta = \pi/2$. When the polarization analyzer is oriented in such a way as to transmit a mixture of two cross-polarized field components, $\theta = \pi/4$ in Fig. 2(b), clearly resolved fringes are observed in the spectrum of the fiber output (point X on the polarization-evolution trajectory shown on the Poincaré-sphere map in Fig. 3(c), visualizing the interference of two temporally separated waveforms polarized along the fast and slow axes of the birefringent fiber [see Figs. 3(a) and 3(b)]. These fringes indicate the coherence of the orthogonal polarization modes at the fiber output, showing that, although PI in our experiments can amplify low-amplitude cross-polarized field components [Figs. 3(c) and 3(d)], as long as the amplitude of the coherent cross-polarized seed is much higher than the amplitude of the noise in this mode, it does not lead to coherence degradation in the orthogonal polarization modes through dramatic noise amplification. Because of dispersion-induced pulse stretching, the polarization modes become decoupled as the peak power in a mode becomes less than P_{cr} [point R in Fig. 3(c), corresponding to a propagation path of 1 cm inside the fiber; see Fig. 3(b)].

The PI dynamics of ultrashort pulses demonstrated in this Letter radically differs from the PI dynamics of cw fields and longer laser pulses. As the peak power of an ultrafast field waveform decreases along the propagation path due to dispersion-induced pulse stretching, polarization dynamics of the optical field is shown to evolve from the behavior typical of PI in the highly nonlinear regime toward the beating dynamics of uncoupled polarization modes, characteristic of low field intensities and cw fields. This interplay of nonlinear-optical dynamics and dispersion is specific to ultrashort pulses, suggesting no direct scaling to longer pulse widths. Moreover, for pulses as long as a few picoseconds, the level of peak powers required for PI-induced vectorial SC generation observed in this Letter translates into fluences close to the fiber breakdown threshold.

This work was supported in part by the Russian Foundation for Basic Research, Welch Foundation (grant A-1801), and Skolkovo Foundation (grant 78). A. M. Z. gratefully acknowledges partial support of his research in Jena through the guest professorship awarded by the Abbe School of Photonics.

References

1. T. B. Benjamin, Proc. R. Soc. Math. Phys. Eng. Sci **299**, 59 (1967).
2. T. Tainuti and H. Washimi, Phys. Rev. Lett. **21**, 209 (1968).
3. G. P. Agrawal, *Nonlinear Fiber Optics* (Academic, 2001).
4. L. Salasnich, A. Parola, and L. Reatto, Phys. Rev. Lett. **91**, 080405 (2003).
5. V. I. Bespalov and V. I. Talanov, JETP Lett. **3**, 307 (1966).
6. P. St. J. Russell, Science **299**, 358 (2003).
7. J. D. Harvey, R. Leonhardt, S. Coen, G. K. L. Wong, J. C. Knight, W. J. Wadsworth, and P. St. J. Russell, Opt. Lett. **28**, 2225 (2003).
8. E. E. Serebryannikov, S. O. Konorov, A. A. Ivanov, M. V. Alfimov, M. Scalora, and A. M. Zheltikov, Phys. Rev. E **72**, 027601 (2005).
9. A. M. Zheltikov, JETP Lett. **85**, 539 (2007).
10. R. J. Kruhlak, G. K. Wong, J. S. Chen, S. G. Murdoch, R. Leonhardt, J. D. Harvey, N. Y. Joly, and J. C. Knight, Opt. Lett. **31**, 1379 (2006).
11. J. M. Dudley, G. Genty, and S. Coen, Rev. Mod. Phys. **78**, 1135 (2006).
12. A. M. Zheltikov, Phys. Uspekhi **49**, 605 (2006).